

Modes of Interannual Tropical Ocean–Atmosphere Interaction—a Unified View. Part III: Analytical Results in Fully Coupled Cases

FEI-FEI JIN* AND J. DAVID NEELIN

Department of Atmospheric Sciences, University of California, Los Angeles, Los Angeles, California

(Manuscript received 24 December 1991, in final form 23 February 1993)

ABSTRACT

The parameter-space dependence of the eigenmodes of the coupled tropical ocean–atmosphere system, linearized about a climatological basic state, is further examined in a stripped-down intermediate coupled model using the formulation derived in Part II of this study to permit analytical treatment for a finite ocean basin. Part II examined the limit of weak coupling and showed the rapid transition to the mixed SST/ocean dynamics modes of Part I, where it was argued that realistically coupled modes are best understood from strong coupling. Here cases with order unity and larger coupling are explored to provide analytical prototypes for the fully coupled case from a system that explicitly treats spatial structure in a finite basin. The coupled dynamics is explored for several regions of parameter space where simplifications are possible, as well as for the transition from the well-separated case to mixed modes.

The case of *surface-layer processes only* provides a simple example of westward-propagating SST modes. Extensive results are given for SST modes in the *fast-wave limit*. In addition to propagating SST modes, stationary, purely growing SST modes exist over a significant range of parameters; these are focused on because of their close relation to the mixed SST/ocean-dynamics modes with standing SST oscillations and subsurface memory. The latter can be thought of as stationary SST modes perturbed by wave dynamics. The east basin trapping exhibited by these modes can be produced even in a zonally homogeneous basic state as the result of east–west asymmetry due to β in both atmosphere and ocean.

An important new case is the *strong-coupling limit* where strongly growing modes dominated by coupled processes are examined. These depend on both SST and ocean-dynamics time scales, but equatorial oceanic wave dynamics in the conventional sense is secondary to coupled processes in the basin interior. Because of this, these strongly growing modes are directly connected to SST modes in the fast-wave limit; extrapolating from the strong-coupling limit toward the fast-wave limit, and vice versa, permits this eigensurface to be pieced together qualitatively. Purely growing modes in the strong-coupling limit can be traced all the way from the fast-wave limit to its converse, the fast-SST limit. This, and the relation of the strongly coupled modes to the SST modes, serves to explain the connection of the eigensurfaces found in Part I and suggests that they must be a very robust feature of the coupled system.

1. Introduction

A great deal about the behavior of the coupled tropical ocean–atmosphere system may be understood in terms of the eigenmodes of the system, linearized about the climatological basic state. In Parts I (Jin and Neelin 1993) and II (Neelin and Jin 1993) of this paper, we examined these coupled modes in a model closely related to that of Zebiak and Cane (1987); a simple atmospheric model coupled to a modified shallow-water ocean with simplified mixed-layer dynamics and a sea surface temperature (SST) equation for an equatorial band, following Neelin (1991, N91 hereafter). In Part

I, we argued on the basis of numerical results that the connection between the various regions of parameter space for the coupled system could be understood in a straightforward manner. In the uncoupled system, one finds two classes of modes: “ocean-dynamics modes,” by which we refer to modes associated with the time scales of subsurface wave dynamics, and SST modes, which are related to the time derivative of the SST equation. Coupled versions of these modes remain distinct in a limit defined in N91 that is useful for understanding their behavior: the *fast-wave limit*, which is obtained when the dynamical adjustment of the ocean by wave dynamics occurs fast compared to the time scale of SST evolution by coupled processes. Part I showed that elsewhere in the coupled parameter space, these modes are not well separated and are best understood as *mixed SST/ocean-dynamics modes*. The modes can be traced as a function of parameter, with the eigenvalues forming continuous complex surfaces in parameter space. These eigensurfaces join at sin-

* Current affiliation: Department of Meteorology, University of Hawaii at Manoa, Honolulu, Hawaii.

Corresponding author address: Dr. Fei-Fei Jin, Department of Atmospheric Sciences, UCLA, 405 Hilgard Ave., Los Angeles, CA 90024-1565.

gularities with degenerate eigenvalues of algebraic multiplicity two or three (we use the abbreviation 2- and 3-degeneracy), so it is possible, for instance, to move continuously from an eigensurface originally characterized as an SST mode to one originally characterized as an ocean-dynamics mode.

To better understand the balances involved in the merger of these modes, in Parts II and III we approach the problem analytically as far as possible. In the realistic case of an ocean basin with finite zonal extent, this requires a formulation in which the boundary conditions associated with wave dynamics and the effects of the finite basin on the atmospheric model may be taken into account in making approximations. In Part II, we made use of results from Cane and Sarachik (1981) and Cane and Moore (1981) to derive a Green's function solution for the response of the ocean component to a wind stress whose complex frequency/growth rate and zonal structure is *internally* determined by the coupled system. Combined with the SST equation and atmospheric model, the eigenvalue problem is thus formulated in terms of integral operators in x that provide a good basis for making approximations.

Our strategy is to obtain analytic or near-analytic results in limits whose regions of validity surround the complicated region where the degeneracies occur. This gives insight into the coupled dynamics that apply in the various regions. In Part II, we examined the *weak coupling limit* and were able, for instance, to argue roughly where in parameter space the transition occurs between weakly modified ocean basin modes and mixed SST/ocean-dynamics modes. Here we examine a number of useful cases for which we can obtain results

at order unity and stronger coupling. After restating the model in section 2, we begin with the relatively simple case of *surface-layer processes only* in section 3. This provides a prototype for the solution method and allows insight into the westward-propagating SST modes found in a number of GCMs. In section 4, we examine the *fast-wave limit* in which we can examine SST modes uniformly from weak to strong coupling. Section 5 introduces the *strong-coupling limit* and the connection of this to the fast-wave limit. This permits us to examine the transition from pure SST modes to strongly coupled modes that have a mixed character. Summary and discussion of these results and connections to Parts I and II are provided in section 6.

2. The model

The model is as in Part II, using the same nondimensionalization and integral formulation of the eigenvalue problem. It assumes linearization about a basic state with mean upwelling and a time dependence $\exp(\sigma t)$ for the perturbations, where σ is the temporal eigenvalue. The linearized SST equation for the equatorial band is

$$\sigma T = a(x)u_e + \gamma(x)h_e - \epsilon_w(x)T + \mu\delta_s b(x)\mathcal{A}_e(T; x), \quad (2.1)$$

where a number of less important terms have been dropped, as discussed in Part II. In particular, horizontal diffusion terms play little role for basin-scale modes at finite coupling. The equatorial values of vertical-mean zonal current above the thermocline and thermocline depth perturbations are given by

$$u_e = -i\mu \left[\int_0^1 \left(\frac{\sin 2\phi x_0}{\sin 2\phi} \right)^{1/2} \mathcal{A}_e(T; x_0) dx_0 (\cos 2\phi(x-1))^{-1/2} \sin 2\phi(x-1) \right. \\ \left. - \int_x^1 \mathcal{A}_e(T; x_0) (\cos 2\phi(x-x_0))^{-1/2} \sin 2\phi(x-x_0) dx_0 \right] \\ h_e = \mu \left[\int_0^1 \left(\frac{\sin 2\phi x_0}{\sin 2\phi} \right)^{1/2} \mathcal{A}_e(T; x_0) dx_0 (\cos 2\phi(x-1))^{1/2} - \int_x^1 \mathcal{A}_e(T; x_0) (\cos 2\phi(x-x_0))^{1/2} dx_0 \right] \quad (2.2)$$

where $\phi = -i(\delta\sigma + r)$ and r is ocean damping.

The atmospheric model $\mathcal{A}(T; x)$ is a linear but nonlocal function of SST, whose y dependence is assumed slow compared to the oceanic radius of deformation. We use a Gill (1980) model, retaining only the zeroth Hermite function in the meridional structure of the forcing, so the equatorial value of the zonal wind stress is given by the simple integral operator:

$$\mathcal{A}_e(T; x) = A_0\epsilon_a \left[\frac{3}{2} \exp(3\epsilon_a x) \int_x^1 \exp(-3\epsilon_a s) T ds \right. \\ \left. - \frac{1}{2} \exp(-\epsilon_a x) \int_0^x \exp(\epsilon_a s) T ds \right] \quad (2.3)$$

where ϵ_a is a nondimensional inverse decay scale proportional to the atmospheric boundary-layer damping rate and boundary conditions of zero anomalous forcing outside of the ocean basin have been used. The nondimensional parameter A_0 is a constant factor required to make the operator order unity for standard values; $A_0 = 15$ is used in all plots, as in Part II.

The coefficients a , γ , ϵ_w , and b in the temperature equation are nondimensional basic-state quantities, scaled to be unity under reasonable conditions. The first three are associated with zonal advection by perturbation currents, thermocline feedback due to vertical advection of subsurface temperature perturbations, and

damping by surface fluxes and mean vertical advection, respectively. The coefficient b is associated with the combined effects of vertical and zonal advection by surface-layer perturbation currents. Their longitudinal dependence is quantitatively important to the coupled modes in the basin but, as in Part II, we mainly consider the special case where these are treated as constant. This facilitates analytical solution and also highlights the spatial structure implied by the finite ocean basin. We find that the most important qualitative behavior of the system, the smooth joining of eigensurfaces associated with oceanic and SST time derivatives, is reproduced even in this very simplified case.

The important parameters of the system as defined in Part II are listed in Table 1 for reference. The relative coupling coefficient measures the strength of the wind stress feedback per unit SST anomaly, relative to standard values, from the atmospheric model. The relative adjustment time coefficient is the ratio of the time scale characterizing dynamical adjustment by equatorial waves, t_c , to the net time scale of SST change by various coupled processes, t_T . The surface-layer coefficient, δ_s , measures the strength of the surface layer effects; specifically, it is the inverse ratio of the coupled time scale of SST change through advection by vertical/meridional and zonal vertical-shear Ekman currents, t_s , to the coupled time scale of SST change through feedbacks involving the thermocline and vertical-mean currents above the thermocline, t_m . An important parameter controlling the atmospheric model spatial structure is the boundary-layer damping rate, ϵ_a , here scaled as a damping length relative to the zonal basin scale. Finally, two damping parameters are important, although we make less explicit use of them: ϵ_T is the net damping of SST anomalies due to surface processes; in the SST equation, (2.1), it is combined with an effective dynamical damping of SST anomalies due to mean upwelling to give a total damping, ϵ_w . Damping processes affecting oceanic dynamics are represented by a Rayleigh friction/Newtonian cooling coefficient, r , in the shallow-water subsystem. Ocean damping is helpful in keeping the fast-wave limit well defined; we always let $r \rightarrow 0$ last when taking sensitive limits. The damping parameters give a simple correspondence between 2-degeneracies and codimension-2 bifurcations, as discussed in Part I.

3. SST modes: Case of surface-layer processes only

It was shown in Part II (section 4b) in the weak-coupling case that several feedback mechanisms tend to destabilize the SST modes, including processes from thermocline depth fluctuations and horizontal and vertical advection by both vertical mean currents and currents associated with the surface layer. These different feedback processes shape SST in very different ways. In this section, we focus on the SST modes in the case of large δ_s , where the feedbacks from advection

TABLE 1. Primary parameters.

μ	relative coupling coefficient
$\delta \equiv t_c/t_T$	relative adjustment time coefficient
$\delta_s \equiv t_m/t_s$	surface-layer coefficient
ϵ_a	damping length scale of atmospheric model
r	damping time scale of shallow-water ocean dynamics
ϵ_T	damping time scale of SST by surface fluxes

and Ekman pumping due to surface-layer processes dominate over feedback processes due to the vertical mean currents and thermocline displacement. The latter will be analyzed in the next section. As discussed in Part II, section 2, the product $b\delta_s$ is order unity if large δ_s is due to weak vertical-mean current processes rather than very strong surface-layer processes.

Dropping the terms in h and u_m from the SST equation gives

$$\sigma T = -\epsilon_w T + b\delta_s \mu \mathcal{A}_e(T; x), \quad (3.1)$$

with \mathcal{A}_e given by the integral operator (2.3); (3.1) is an integral equation describing the coupled SST modes. As discussed in section 3, we treat the potentially x -dependent basic-state coefficients, ϵ_w and b , as constant both for simplicity and to highlight spatial structure inherent to the ocean basin.

To solve (3.1), we first invert the integral operator from the atmospheric model to get a differential equation

$$(\sigma + \epsilon_w)(\partial_x^2 - 2\epsilon_a \partial_x - 3\epsilon_a^2)T = -2b\delta_s \mu \epsilon_a A_0 \partial_x T. \quad (3.2)$$

For a solution of the form

$$T = T_k e^{kx + \sigma t}, \quad (3.3)$$

the resulting dispersion relation is

$$(\sigma + \epsilon_w)(k^2 - 2\epsilon_a k - 3\epsilon_a^2) = -2b\delta_s \mu \epsilon_a A_0 k. \quad (3.4)$$

For each σ , (3.4) gives two roots for k . Thus, we have a formal solution

$$T = \left(\sum_{i=1}^2 T_{k_i} e^{k_i x} \right) e^{\sigma t}. \quad (3.5)$$

We then substitute (3.5) with (3.4) back to (3.1) and (2.3), which already has the boundary conditions built into the integral operator. In this case, the boundary conditions are those required by the atmospheric model, that is, no SST anomalies outside the basin. The limits of integration associated with these boundaries in (2.3) give two terms with x dependencies $e^{3\epsilon_a x}$ and $e^{-\epsilon_a x}$ in addition to the eigenstructure x dependence $e^{ik_1 x}$ and $e^{ik_2 x}$. The boundary conditions then appear in the requirement that the coefficients of $e^{3\epsilon_a x}$ and $e^{-\epsilon_a x}$, after integration of (3.5) and (2.3) in (3.1), be zero. The dispersion relation (3.4) can be derived by this same method; our device of passing via

the differential equation (3.2) is merely a convenience that makes the number of independent x structures required in (3.5) immediately apparent. The boundary conditions yield two quantization conditions required for a nontrivial solution:

$$\sum_{i=1}^2 \frac{e^{k_i}}{-3\epsilon_a + k_i} T_{k_i} = 0$$

$$\sum_{i=1}^2 \frac{T_{k_i}}{\epsilon_a + k_i} = 0, \tag{3.6}$$

which give an eigenvalue equation:

$$\begin{vmatrix} (k_1 - 3\epsilon_a)^{-1} \exp(k_1) & (k_2 - 3\epsilon_a)^{-1} \exp(k_2) \\ (\epsilon_a + k_1)^{-1} & (\epsilon_a + k_2)^{-1} \end{vmatrix} = 0, \tag{3.7}$$

where k_1 and k_2 are the roots of (3.4). Thus, (3.7) determines the temporal eigenvalue σ , while (3.4) yields the spatial eigenvalues and (3.6) determines the eigenvector (T_{k_i}), to complete the SST mode solution (3.5).

When ϵ_a is small, that is, the atmospheric damping radius is large compared to the basin length, a fully analytical solution of σ from (3.7) is possible. We apply the small ϵ_a approximation to the structure of the atmospheric operator, retaining only terms to zeroth order in ϵ_a , but do not make this assumption for the magnitude, retaining $\epsilon_a A_0$ where it multiplies coupling. From (3.4), we then have

$$k_1 \approx -2b\delta_s\mu\epsilon_a A_0(\sigma + \epsilon_w)^{-1} + O(\epsilon_a)$$

$$k_2 \approx O(\epsilon_a^2). \tag{3.8}$$

Thus, (3.7) can be approximately written as

$$e^{k_1} = -\frac{1}{3} = e^{-\ln 3 - i\pi} \tag{3.9}$$

or

$$k_1 = -\ln 3 + i(2n - 1)\pi, \quad n = 1, 2, 3, \dots$$

$$\sigma = -\epsilon_w + \frac{2b\delta_s\mu\epsilon_a A_0[\ln 3 + (2n - 1)i\pi]}{(\ln 3)^2 + (2n - 1)^2\pi^2} \tag{3.10}$$

where $n = 0, -1, -2, \dots$ solutions just give the complex conjugates. The solution is thus

$$T = T_{k_1} \exp \left[-x \ln 3 + \left(\frac{2b\delta_s\mu\epsilon_a A_0 \ln 3}{(\ln 3)^2 + (2n - 1)^2\pi^2} - \epsilon_w \right) t \right]$$

$$\times \exp \left[i(2n - 1)\pi \left(x + \frac{2b\delta_s\mu\epsilon_a A_0}{(\ln 3)^2 + (2n - 1)^2\pi^2} t \right) \right]$$

$$+ O(\epsilon_a). \tag{3.11}$$

Since b is normally positive, when μ is large enough, $\sigma_r \equiv \text{Re}(\sigma)$ can become positive, yielding growing,

westward-propagating SST modes. The dispersion relation, (3.10), shows clearly that the most unstable mode has largest spatial scale and lowest frequency. There is slight eastward-decaying factor due to 3^{-x} giving an amplitude change of $1/3$ over the basin.

In the general case of ϵ_a not small, using the relation

$$k_2 = -3\epsilon_a^2/k_1, \tag{3.12}$$

which is obtained from (3.4), we can easily obtain a numerical solution for roots of k_1 satisfying the eigenvalue equation (3.7). We define for convenience

$$f(k_1, \epsilon_a) = \frac{-k_1\epsilon_a A_0}{k_1^2 - 2\epsilon_a k_1 - 3\epsilon_a^2} \tag{3.13}$$

such that

$$\sigma + \epsilon_w = 2b\delta_s\mu f(k_1, \epsilon_a) \tag{3.14}$$

so that $f(k_1, \epsilon_a)$ summarizes the k_1 and ϵ_a dependence of the eigenvalue. Physically, $f(k_1, \epsilon_a)$ describes the relation of SST anomaly and wind stress anomaly. Because the k_1 solution is always complex, f is also complex, giving the phase difference between the two fields, which produces propagating modes; $\text{Re}(f)$ represents the rate of reinforcement of an SST anomaly by the wind stress-induced surface-layer feedback. To the extent that stress anomalies are in phase with SST anomalies, the resulting vertical and zonal advection anomalies will produce growth. To the extent that positive stress anomalies occur out of phase (to the west) of positive SST anomalies, the resulting advection causes westward propagation. The mechanisms are qualitatively similar to the periodic disturbance case (for which k_1 would be specified and pure imaginary) except that the modes must satisfy the quantization conditions (3.7).

Although the dependence of k_1 on ϵ_a has to be numerically evaluated, (3.14) gives an exact analytical expression for the eigenvalue σ once we get $k_1(\epsilon_a)$ for different modes, analogous to (3.10). Figures 1a,b show $f(k_1, \epsilon_a)$ and k_1 , respectively, as a function of ϵ_a for the gravest mode. As ϵ_a increases, the imaginary part of k_1 increases; that is, the spatial scale of the SST mode becomes smaller. The eastward-decay factor due to $\text{Re}(k_1)$ also diminishes, while the eastward-amplifying k_2 increases. This results in a mode with considerable amplitude throughout the basin.

As ϵ_a increases, two effects occur in $f(k_1, \epsilon_a)$. Because the effect of ϵ_a on coupling strength is included in Fig. 1, the growth rate and frequency become small as ϵ_a becomes small. Aside from this linear factor, the effect of ϵ_a in the atmospheric model structure tends to reduce both growth rate and frequency so the net effect is modest away from the smallest ϵ_a range. The imaginary part of k_1 increases substantially with ϵ_a , as does k_2 according to (3.12). The gravest spatial mode is still the most unstable and lowest-frequency mode, as may be expected from (3.13).

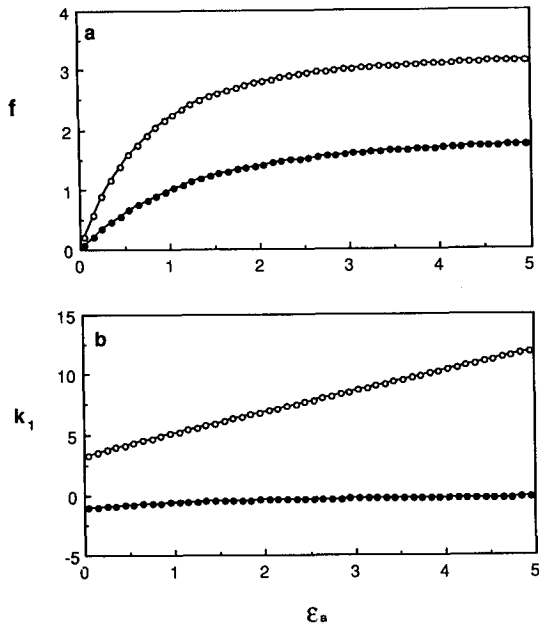


FIG. 1. Eigenvalue and wavenumber dependence on inverse atmospheric damping length, ϵ_a , of the gravest westward-propagating SST mode (surface-layer-only case). (a) Factor for eigenvalue dependence, $f(k_1, \epsilon_a)$; real part (scaled growth rate tendency): solid circles, imaginary part (scaled frequency): open circles. (b) One of the two complex wave numbers, k_1 ; real part: solid circles, imaginary part: open circles.

Once the eigenvalues are obtained, we can derive the eigenstructure very easily. If we use (3.4) and (3.7), the eigenvector is

$$\hat{T}(x, \sigma) = (\epsilon_a + k_1)e^{k_1 x} - (\epsilon_a + k_2)e^{k_2 x} \quad (3.15)$$

aside from an arbitrary amplitude factor. The value of k_2 is obtained by using (3.12), and it has a small positive real part that gives a slight eastward amplification. Figure 2 shows a time-longitude plot that combines this eigenvector with the oscillatory part of $e^{\sigma t}$. The westward propagation is very similar to the results obtained in Part I except that the mode is less trapped in the eastern part of the basin. The inhomogeneity in the basic state of Part I is thus apparently quantitatively important for the east basin trapping of westward-propagating SST modes for this case where the thermocline feedback is neglected.

While the modes discussed here are simpler than those seen in Part I and much simpler than the westward-propagating modes found in various GCM experiments (Meehl 1990; Neelin 1990; Lau et al. 1991), they provide a useful prototype for westward-propagating SST modes in the case where surface-layer processes dominate. When the thermocline feedback term is included but is not too strong, we know from N91 and Part I that similar modes may be found. As the relative importance of the surface-layer processes is weakened by reducing δ_s , the westward propagation is

slowed and eventually the modes become stationary (or even eastward propagating) due to the competing effects of the thermocline feedback. Section 4b of Part II shows this effect in the weak-coupling case; rather than repeat the analysis of this transition, we turn directly to the case of an inactive surface layer in the following sections.

4. SST modes in the fast-wave limit and its first-order correction

When the thermocline feedback and advection by vertical-mean currents are taken into account, complication immediately follows as the subsurface dynamics becomes involved. Analysis of SST modes at strong coupling is simplified in the fast-wave limit since the time scales of wave dynamics are not important. By examining also the first-order correction to the fast-wave limit, we can obtain insight into the behavior of the modes near this limit and into its accuracy in approximating modes at realistic parameters. Of particular interest is the stationary, eastward-trapped SST mode found in Part I and examined at low coupling in section 4b of Part II. For simplicity, we let $\delta_s = 0$; that is, we turn off the surface-layer feedback processes due to Ekman pumping and Ekman flow advection that are discussed in section 5. The SST equation (2.1) becomes

$$\sigma T = au_e + \gamma h_e - \epsilon_w T. \quad (4.1)$$

In the fast-wave limit, where δ is small, the general integral expressions of u_e and h_e (2.2) can be much simplified provided $\sigma\delta \ll 1$, the region of validity of which is discussed in section 3 of Part II. Expanding the Green's function in terms of δ and retaining only the terms first order and larger, under the assumption $\delta\sigma \ll 1$, we obtain

$$\begin{aligned} u_e(x, \sigma) &\approx -2(\delta\sigma + r)\mu \left[(x-1) \int_0^1 \sqrt{x_0} \mathcal{A}_e(T; x_0) dx_0 \right. \\ &\quad \left. - \int_x^1 (x-x_0) \mathcal{A}_e(T; x_0) dx_0 \right] \\ h_e(x, \sigma) &\approx \mu \left[\int_0^1 \sqrt{x_0} \mathcal{A}_e(T; x_0) dx_0 \right. \\ &\quad \left. - \int_x^1 \mathcal{A}_e(T; x_0) dx_0 \right]. \quad (4.2) \end{aligned}$$

This approximation satisfies the boundary condition $u_e(1, \sigma) = 0$ and becomes exactly the Sverdrup balance as $\sigma \rightarrow 0$, the fast-wave limit. The differential equations corresponding to (4.2) are just

$$\begin{aligned} \frac{\partial}{\partial x} h_e &= \mu \mathcal{A}_e(T; x) \\ \frac{\partial^2}{\partial x^2} u_e &= -2(\delta\sigma + r)\mu \mathcal{A}_e(T; x). \quad (4.3) \end{aligned}$$

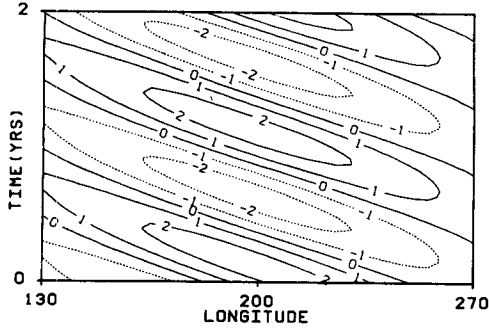


FIG. 2. Time-longitude dependence along the equator of the SST component of the westward-propagating SST mode. Surface-layer-only case with $\epsilon_a = 3.0$, $\epsilon_w = 1.0$, $\mu = 2/3$; arbitrary units.

This is a first-order correction of the $\delta = 0$ fast-wave limit used in N91.

The system (4.1)–(4.2) again forms an integral equation for the SST modes. Following the same procedure used in section 3, inverting this integral equation into a differential form, we obtain a dispersion relation

$$(\sigma + \epsilon_w)(k^2 - 2\epsilon_a k - 3\epsilon_a^2)k^2 = -2k\epsilon_a A_0 \mu [\gamma k - 2a(\delta\sigma + r)]. \quad (4.4)$$

For a given value of σ , (4.4) gives four roots for k , with one of them zero, which together govern spatial dependence. Thus, a formal solution will be

$$T = (T_0 + \sum_{i=1}^3 e^{k_i x} T_{k_i}) e^{\sigma t}. \quad (4.5)$$

Substituting this solution back into (4.1) and (4.2), which contains the boundary conditions, we can derive the set of equations for the temporal eigenvalue σ and the eigenvector $(T_0, T_{k_1}, T_{k_2}, T_{k_3})^T$.

Similar to the case discussed in the last section, the integral operator in the atmospheric model gives two terms in $e^{3\epsilon_a x}$ and $e^{-\epsilon_a x}$ after integration using (4.5). Eliminating these two terms gives two equations very similar to (3.6). The boundary conditions built into (4.2) give two additional terms with linear and constant x dependences. Eliminating the term in x and balancing the constant term with the constant term in the eigenstructure (4.5) yield two more equations. Thus, we obtain four linear equations for T_0 and T_{k_i} as follows:

$$\begin{aligned} \sum_{i=1}^3 \frac{e^{k_i}}{3\epsilon_a - k_i} T_{k_i} + \frac{1}{3\epsilon_a} T_0 &= 0 \\ \sum_{i=1}^3 \frac{T_{k_i}}{\epsilon_a + k_i} + \frac{1}{\epsilon_a} T_0 &= 0 \\ \sum_{i=1}^3 \frac{B(k_i)}{k_i^2} e^{k_i} T_{k_i} &= \frac{\sigma + \epsilon_w}{2(\delta\sigma + r)a\epsilon_a A_0 \mu} T_0 \\ \sum_{i=1}^3 \left(g(k_i) - \frac{e^{k_i}}{k_i} \right) B(k_i) T_{k_i} &= 0 \end{aligned} \quad (4.6)$$

where

$$\begin{aligned} B(k_i) &= \frac{3}{2(3\epsilon_a - k_i)} - \frac{1}{2(\epsilon_a + k_i)} \\ g(k_i) &= \int_0^1 \sqrt{x} e^{k_i x} dx. \end{aligned} \quad (4.7)$$

Here $B(k_i)$ comes from the atmospheric operator, and $g(k_i)$ from the constant of integration in the thermocline solution (4.2). For a nontrivial solution, the 4×4 matrix multiplying the eigenvector in (4.6) must have zero determinant, yielding a transcendental equation for σ that generally must be solved numerically. However, the limiting case $\delta = 0$, the fast-wave limit, is more easily solved, especially when we also consider small oceanic damping, taking $\delta \rightarrow 0$ first, then $r \rightarrow 0$. The dispersion relation (4.4) becomes

$$(\sigma + \epsilon_w)(k^2 - 2\epsilon_a k - 3\epsilon_a^2) = -2\mu\gamma\epsilon_a A_0 \quad (4.8)$$

and the eigenvalue equation (4.6) becomes for this case

$$\begin{aligned} \sum_{i=1}^2 \frac{e^{k_i}}{3\epsilon_a - k_i} T_{k_i} + \frac{1}{3\epsilon_a} T_0 &= 0 \\ \sum_{i=1}^2 \frac{T_{k_i}}{\epsilon_a + k_i} + \frac{T_0}{\epsilon_a} &= 0 \\ \sum_{i=1}^2 \left(g(k_i) - \frac{e^{k_i}}{k_i} \right) B(k_i) T_{k_i} &= \frac{\sigma + \epsilon_w}{\gamma\mu\epsilon_a A_0} T_0. \end{aligned} \quad (4.9)$$

Although in general the limit is sensitive to the ordering and should be justified as an approximation to the case of small r , in this case it is not. The same set of equations can be obtained either by taking the limit $\delta \rightarrow 0$ and $k_3 \rightarrow 4\epsilon_a A_0 \mu a r [2\epsilon_a A_0 \mu \gamma - 3\epsilon_a^2(\sigma + \epsilon_w)]^{-1}$ in (4.6) or by simply directly integrating (4.1) with (4.2) under the condition $\delta = 0$ and $r = 0$.

Again using the special case where ϵ_a is small to simplify the structure, without assuming small magnitude for the atmospheric operator, we have $k_1 = -k_2 = i\hat{k}$, so the eigenvalue equation can be written as

$$\begin{aligned} F(\hat{k}) &= \left(e^{i\hat{k}} + \frac{1}{3} \right) (g(-\hat{k}) - ie^{-i\hat{k}} \hat{k}^{-1}) \\ &\quad - \left(e^{-i\hat{k}} + \frac{1}{3} \right) (g(\hat{k}) + ie^{i\hat{k}} \hat{k}^{-1}) = 0 \\ g(\hat{k}) &= \int_0^1 \sqrt{x} e^{i\hat{k}x} dx. \end{aligned} \quad (4.10)$$

It is easy to show there is no root for $F(\hat{k})$ when \hat{k} is pure imaginary. There is a set of pure real \hat{k} solutions:

$$\hat{k} \approx \left\{ \begin{aligned} (k_{01} + 2n\pi) \\ (k_{02} + 2n\pi) \end{aligned} \right\}, \quad n = 0, 1, 2, \dots \quad (4.11)$$

that can be seen clearly in Fig. 3. Here k_{01} and k_{02} are the first two roots of equation (4.9), which are obtained numerically. The eigenvalues thus are

$$\sigma + \epsilon_w \approx \frac{2\gamma\mu}{(k_{0i} + 2n\pi)^2}$$

$$i = 1, 2, \quad n = 0, 1, 2, \dots \quad (4.12)$$

Clearly the gravest modes $n = 0, i = 1, 2$ are the most unstable. They exhibit pure growth when coupling is strong enough to overcome the damping in the SST equation.

Because ϵ_a affects the phase relation between SST and wind stress, the stationarity of these SST modes may be expected to depend on this parameter. In the numerical results of Part I, it was noted that the stationary SST mode is eastward trapped, and that for large ϵ_a , the stationary SST mode becomes eastward propagating for the case where the thermocline feedback dominates. With $\epsilon_a \neq 0$, (4.8) may be written

$$k_1 = \epsilon_a + i[2\gamma\mu\epsilon_a A_0(\sigma + \epsilon_w)^{-1} - 4\epsilon_a^2]^{1/2},$$

$$k_2 = 2\epsilon_a - k_1 \quad (4.13)$$

from which it is clear that for nonzero ϵ_a (but small enough not to qualitatively affect the eigenvalue) the spatial eigenvalues k_1, k_2 have a positive real part that traps the mode in the eastern part of the basin with an atmospheric damping length decay scale. This eastward trapping could be further enhanced by longitudinal dependence of upwelling and other parameters but arises in this simple case from the east-west asymmetry in the atmospheric model alone. The lack of real k_1, k_2 roots for (4.10) leads one to further anticipate from (4.13) that as ϵ_a becomes large, the eigenvalue will have to become complex. This is borne out by numerical solutions of (4.9), shown in Fig. 4. Similar to the case of (3.11), we define for convenience

$$\hat{f}(k_1; \epsilon_a) = -\epsilon_a A_0 (k_1^2 - 2\epsilon_a k_1 - 3\epsilon_a^2)^{-1} \quad (4.14)$$

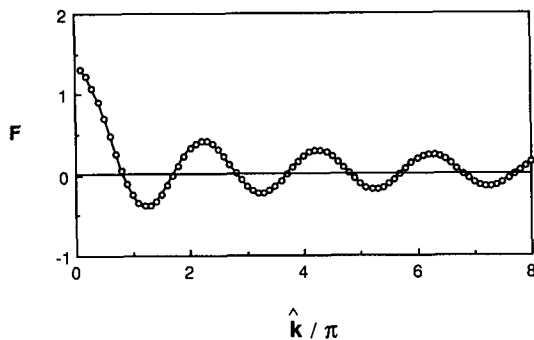


FIG. 3. Graphic solution of (4.10): zeros of $F(\hat{k})$ give eigenvalues in the fast-wave limit for $\epsilon_a = 0.0$.

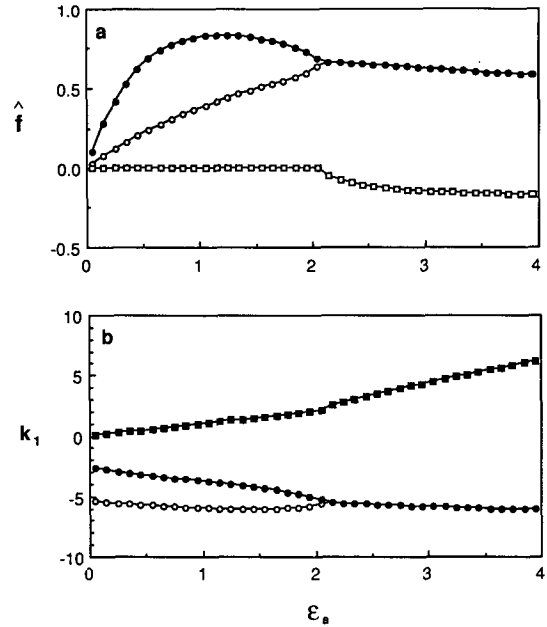


FIG. 4. Eigenvalue and wavenumber dependence on inverse atmospheric damping length, ϵ_a , of the two gravest SST modes (fast-wave limit case with $\delta_s = 0$). (a) Factor for eigenvalue dependence, $\hat{f}(k_1, \epsilon_a)$; real part (scaled growth rate tendency): solid circles (gravest mode) and open circles (second mode), imaginary part (scaled frequency): open squares. (b) One of the three complex wavenumbers, k_1 ; imaginary part: solid circles (gravest mode) and open circles (second mode), real part: solid squares.

such that

$$\sigma + \epsilon_w = 2\gamma\mu\hat{f}(k_1; \epsilon_a) \quad (4.15)$$

so that $\hat{f}(k_1; \epsilon_a)$ summarizes the k_1, ϵ_a dependence of the eigenvalue. Figure 4 shows $\hat{f}(k_1; \epsilon_a)$ and k_1 for the two gravest modes. The gravest mode is the most unstable and, when ϵ_a is not too large, all modes are stationary. As ϵ_a becomes sufficiently large (i.e., for an atmospheric damping length less than about half the basin width), the two gravest modes, which were purely growing at smaller ϵ_a , merge at a 2-degeneracy and produce an oscillatory pair. Here $\hat{f}(k_1; \epsilon_a)$ describes the relation of the SST anomaly and the thermocline depth fluctuation. In the range where ϵ_a is not too large and $\hat{f}(k_1; \epsilon_a)$ is real, there is no phase difference between SST and h so the feedback from the thermocline fluctuation yields a purely growing SST mode. In the large- ϵ_a range, where $\hat{f}(k_1; \epsilon_a)$ becomes complex, the oscillatory modes are associated with zonal and temporal phase lags of h and T . This latter case has mechanisms qualitatively similar to the simple zonally periodic case of N91, with the basin effects yielding eastward trapping. The stationary case—and the transition to it—is new and is of great interest.

Each value of σ has two associated values of k contributing to the eigenstructure. In addition, there is a spatially constant component, T_0 , in the SST structure.

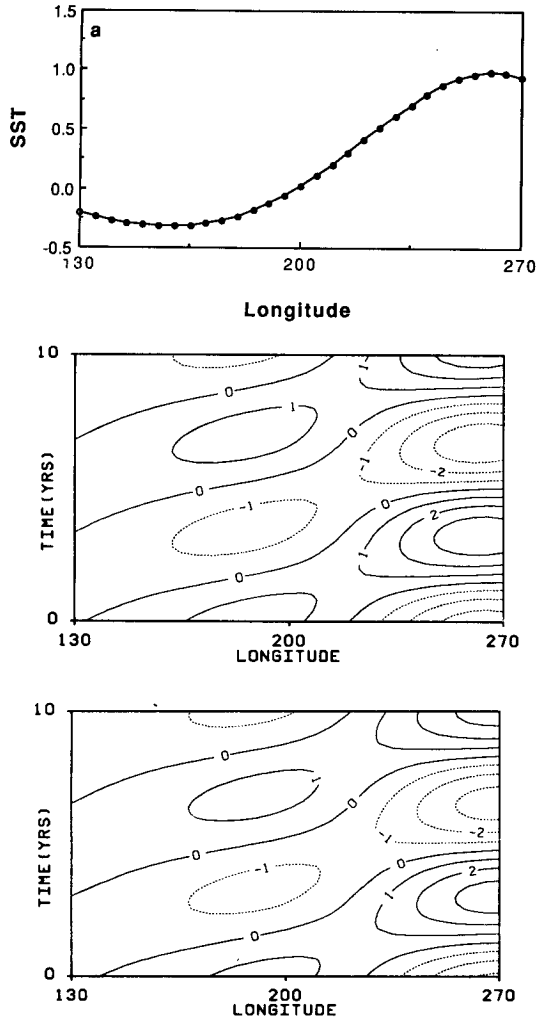


FIG. 5. Eigenvectors for SST modes in the fast-wave limit. (a) SST structure for stationary mode for $\epsilon_a = 1.5$. (b) Time-longitude dependence along the equator of SST component of eastward-propagating SST mode with $\epsilon_a = 2.5$, $\epsilon_w = 1.0$, $\mu = 0.75$. (c) As in (b) but for h component. Units normalized for SST; h in units of $2\mu|f|$.

Thus, the oscillatory mode will potentially have eastward-propagating, westward-propagating, and standing components. For a given eigenvalue, the eigenvector can be written as

$$\hat{T} = 1 + T_{k_1} e^{k_1 x} + T_{k_2} e^{k_2 x} \quad (4.16)$$

with

$$\begin{bmatrix} T_{k_1} \\ T_{k_2} \end{bmatrix} = - \begin{bmatrix} (3\epsilon_a - k_1)^{-1} \exp(k_1) & (3\epsilon_a - k_2)^{-1} \exp(k_2) \\ (\epsilon_a + k_1)^{-1} & (\epsilon_a + k_2)^{-1} \end{bmatrix}^{-1} \times \begin{bmatrix} (3\epsilon_a)^{-1} \\ \epsilon_a^{-1} \end{bmatrix}. \quad (4.17)$$

When σ is real, k_1 and k_2 are complex conjugate and thus so are T_{k_1} and T_{k_2} , giving real \hat{T} . When σ is complex, the first term in (4.16) plus part of the second pair of terms give a standing component to the oscillation, while the remainder of the second pair yields an eastward-propagating component. The eastward-propagating part is more evident and the mode is more strongly trapped to the east as ϵ_a increases. Figure 5a shows SST structure for the stationary mode and Figs. 5b,c show the time-longitude diagram for this eastward-propagating mode, respectively. East basin trapping in both cases is clearly demonstrated even without any inhomogeneity in the basic state.

One of the important factors that results in this trapping is the exponential x dependence due to ϵ_a . However, even in case of small ϵ_a , the eigenstructure of SST still has east basin dominance. Using (4.16) and letting $\epsilon_a \rightarrow 0$, the eigenvector of SST can be written (up to an arbitrary factor) as

$$\hat{T} = 3 \cos[(k_{0_i} + 2n\pi)(x - 1)] + \cos[(k_{0_i} + 2n\pi)x]. \quad (4.18)$$

The factor of 3 is a result of the east-west asymmetry in the atmosphere model due to β (associated with damped Kelvin and Rossby wave structure). For the gravest mode ($n = 0$, $i = 1$), $k_{0_i} \approx 2.65$, so in the west basin, the two terms in \hat{T} tend to cancel, while in the east they do not. This gives a strong dominance of SST amplitude in the east basin. In this case, the factor of 3 from the atmosphere is crucial in producing the asymmetry while the value of k_{0_i} , which is determined by boundary conditions, selects east basin dominance. This effect may be visualized in physical terms by recalling that for a steady, large-scale zonal wind stress, the thermocline response is larger in the east than in the west; for example, for the spatially constant case, $h = 0$ occurs one-third of the way across the basin (Cane and Sarachik 1981). On the other hand, for a large-scale SST anomaly, the dominant wind response is slightly to the west of the SST. A mode with eastward-enhanced SST thus results from the feedback between greater thermocline response to the east of the stress and greater stress response to the west of the SST.

A priori, one would expect east-west asymmetry due to β in either atmosphere or ocean to be sufficient to introduce asymmetry in the eigenfunctions. However, in the above case, asymmetry in both ocean and atmosphere is required. We can consider a symmetric version of the atmospheric model (corresponding to eastward- and westward-damped gravity waves) by simply dropping the factor of 3 in (2.3). For this atmospheric model, for the case of $\epsilon_a \rightarrow 0$ the factor of 3 in (4.18) disappears. Furthermore, in the $\epsilon_a \neq 0$ case, atmospheric damping no longer has an exponential trapping effect in k_1 and k_2 . The eigenstructure becomes simply

$$\begin{aligned} \hat{T} &= \cos[k_n(x - 1) - \psi(k_n)] \\ &\quad + \cos[k_n x + \psi(k_n)] + \text{const} \\ \psi(k_n) &= \tan^{-1}(\epsilon_a k_n^{-1}), \end{aligned} \quad (4.19)$$

where k_n are pure real. The effect of ϵ_a creates no trapping and the solution is symmetric in the basin [i.e., under the transformation $x \rightarrow (1 - x)$]. Although formally the equations are not invariant under this transformation due to east–west asymmetry in the ocean model, for $r = 0$ and $\delta = 0$, symmetry is broken only by the introduction of a constant term due to oceanic boundary conditions. For antisymmetric stress distributions, this constant is zero. Thus solutions with symmetric SST, producing antisymmetric stress and hence symmetric thermocline feedback, are consistent and exhibit symmetry properties despite β in the ocean.

A similar effect occurs when the east–west asymmetry is retained in the atmosphere but is removed in the ocean by using a nonrotating gravity wave ocean that, for $r = 0$, $\delta \rightarrow 0$, obeys a “Sverdrup balance” (in the sense that thermocline slope balances wind stress as in the true Sverdrup balance) and conserves mass at each latitude. For the case of $\epsilon_a \rightarrow 0$, the atmosphere breaks east–west symmetry only through a spatially constant term. For antisymmetric SST distributions, this constant is zero. Eigenfunctions have antisym-

metric SST, symmetric stress, and antisymmetric thermocline structure. The spatial eigenvalues, $\{k = n\pi, n = 1, 2, \dots\}$ are not too different from the solutions to (4.11).

Introduction of nonzero ϵ_a removes these symmetry properties even for the case of a symmetric ocean. For realistic parameter values, the effects of r and $|\delta\sigma|$ near the bifurcation will tend to be much less important than those of ϵ_a . Thus, while east–west asymmetry in both atmosphere and ocean contributes to producing east basin trapping, it is fair to characterize the atmosphere as the more important of the two.

Understanding this east basin trapping for the stationary mode in this simple case is useful because this property carries over smoothly to the eastward-propagating case when ϵ_a is changed, to the westward-propagating case when δ_s is increased, and to the wave-dependent oscillating mixed SST/ocean-dynamics mode when δ is increased (for μ not too large).

Turning to the first-order correction to the fast-wave limit, when $\delta \neq 0$, we can construct the eigenvector for a given eigenvalue as follows:

$$\begin{aligned} \hat{T} &= 1 + T_{k_1} \exp(k_1 x) + T_{k_2} \exp(k_2 x) \\ &\quad + T_{k_3} \exp(k_3 x) \end{aligned} \quad (4.20)$$

with

$$\begin{bmatrix} T_{k_1} \\ T_{k_2} \\ T_{k_3} \end{bmatrix} = - \begin{bmatrix} (3\epsilon_a - k_1)^{-1} e^{k_1} & (3\epsilon_a - k_2)^{-1} e^{k_2} & (3\epsilon_a - k_3)^{-1} e^{k_3} \\ (\epsilon_a + k_1)^{-1} & (\epsilon_a + k_2)^{-1} & (\epsilon_a + k_3)^{-1} \\ B(k_1) e^{k_1} k_1^{-2} & B(k_2) e^{k_2} k_2^{-2} & B(k_3) e^{k_3} k_3^{-2} \end{bmatrix}^{-1} \begin{bmatrix} (3\epsilon_a)^{-1} \\ (\epsilon_a)^{-1} \\ \frac{\sigma + \epsilon_w}{2\delta\sigma a \mu \epsilon_a A_0} \end{bmatrix}. \quad (4.21)$$

When σ is real, k_1 and k_2 are still complex conjugates and k_3 is real, and thus T_{k_1} and T_{k_2} are complex conjugates, while T_{k_3} is real.

As long as the coupling is not too large, the stationary SST mode solutions in the fast-wave limit are very robust as the time scale ratio δ is increased from zero toward order one, as shown in Fig. 6. This is produced using the first-order correction to the fast-wave limit, (4.6), and the dispersion relation (4.4). Note that σ is not necessarily linear in δ but that, even for quite strong coupling, $\mu = 1$ in this case, there is little change relative to the fast-wave limit. The first-order effects of the wave time scales on the SST mode are small and the SST modes maintain their fast-wave limit behavior to order-one values of δ . However, it should be pointed out that sensitivity to δ also depends on a , which governs the strength of the zonal advection feedback; the larger a is, the smaller the range of δ for which this approximation remains valid.

In the case of the regime of eastward-propagating SST modes, as δ is increased, we find that the propagating mode actually becomes a stationary, pure growth

mode again as shown in Fig. 7. The SST structures for stationary modes in both Fig. 6 and Fig. 7 are shown in Fig. 8. They are qualitatively similar to the structure in Fig. 5b.

Rewriting (4.3) as

$$\begin{aligned} \sigma[k(k^2 - 2\epsilon_a k - 3\epsilon_a^2) - 4a\mu\delta] \\ = -[\epsilon_w k(k^2 - 2\epsilon_a k - 3\epsilon_a^2) + 2\gamma k\mu] \end{aligned} \quad (4.22)$$

we see that the range of validity of the fast-wave limit will change as the coupling becomes very large. As expected, the region of validity of the fast-wave limit depends on the product $\mu\delta$; the larger μ , the smaller the range of δ for which this limit is applicable. It is also clear from (4.22) that it is the gravest SST modes that are the first to be affected as coupling is increased. Although there is only a single temporal eigenvalue in (4.22), the physical properties of the mode change as μ is increased for fixed nonzero δ . From a mode that is clearly identifiable as an SST mode, there is a continuous transformation to a mode that is strongly dependent on δ in the limit of strong coupling. This per-

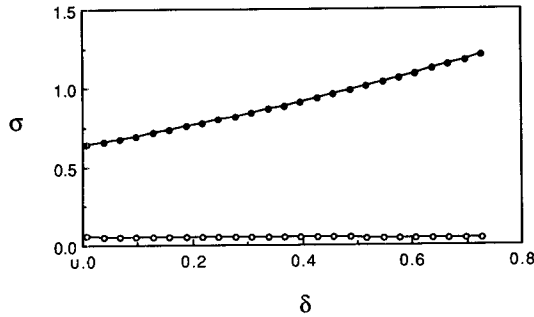


FIG. 6. Growth rate of the gravest two stationary SST modes vs δ for the first-order correction to the fast-wave limit with $a = 1.0$, $\gamma = 1.0$, $\epsilon_w = 1.0$, $\epsilon_a = 1.5$, $\mu = 1.0$. Solid (open) circles for the first (second) mode.

mits us to see the continuous connection between the SST mode and oceanic mode eigensurfaces observed in the numerical results. The coefficient a indicates that the connection occurs at this order through the Gill–Hirst mechanism due to the $u'_m \bar{T}_x$ term of the SST equation. Connection through the thermocline feedback term would enter at higher order in δ .

Although (4.22) indicates that the range of δ for which the first-order correction to the fast-wave limit is a good approximation becomes smaller for large μ , we know from the numerical results that the mode does not undergo strong changes even as oceanic time derivatives become important at strong coupling. To better understand this linkage of the SST mode and oceanic mode eigensurfaces, we turn to an examination of the strong-coupling limit.

5. The strong-coupling limit

In Part II, we examined how the free ocean basin modes arising from the subsurface oceanic wave dynamics can be destabilized and strongly modified through coupling. Although this gives insight into the relation between an ocean basin mode and the oscillatory, nonpropagating mixed SST/ocean-dynamics mode found numerically in Part I, we still lack understanding of why this oscillatory mode connects to a nonoscillatory, strongly growing mode at strong coupling, and how this in turn connects to an SST mode at the fast-wave limit. In this section we apply approximations appropriate to growing modes in the strong-coupling limit to the Green's function derived in section 2 and examine the physical balances of the resulting system and the connection to the fast-wave limit. For further simplification, we again consider the case of an inactive surface layer, $\delta_s = 0$.

Inspection of the coupled system suggests that as coupling becomes large, for finite δ , the balances in the shallow-water ocean component must involve large $|\delta\sigma|$ compensating for the large coupled feedback through the wind stress. To simplify (2.2), we need to

consider also the behavior of the real part of σ . We are interested in the growing eigenmodes and we know from numerical experience that $\text{Re}(\delta\sigma) \gg 1$ for large μ is a reachable condition, appropriate to these modes. As we will see, this assumption is self-consistent with the solutions obtained under it. The approximations made here are more specifically valid under the condition $\text{Re}(\delta\sigma) + r \gg 1$, so if oceanic damping is strong, the same balances can apply for modes with near-neutral growth rates. This is very relevant to the discussion of the bifurcations of the system, but because r is easily reintroduced by shifting the eigenvalues appropriately, we drop it for the time being.

Under this condition, we make the following functional approximations:

$$\begin{aligned} \sinh 2\delta\sigma x &\approx \frac{1}{2} e^{2\delta\sigma x} \\ [\cosh 2\delta\sigma(x-1)]^{-1/2} \sinh 2\delta\sigma(x-1) &\approx \frac{1}{\sqrt{2}} [-e^{\delta\sigma(1-x)} + e^{-3\delta\sigma(1-x)}] \\ [\cosh 2\delta\sigma(x-1)]^{1/2} &\approx \frac{1}{\sqrt{2}} [e^{\delta\sigma(1-x)} + e^{-3\delta\sigma(1-x)}]. \end{aligned} \quad (5.1)$$

The leading behavior for $u_e(x, \sigma)$ and $h_e(x, \sigma)$ thus becomes

$$\begin{aligned} u_e(x, \sigma) &\approx \frac{1}{\sqrt{2}} \left(\int_0^1 e^{-\delta\sigma(1-x_0)} \mathcal{A}_e(T; x_0) dx_0 \right) \\ &\quad \times [e^{\delta\sigma(1-x)} - e^{-3\delta\sigma(1-x)}] - \frac{1}{\sqrt{2}} \int_x^1 \mathcal{A}_e(T; x_0) \\ &\quad \times [e^{\delta\sigma(x_0-x)} - e^{-3\delta\sigma(x_0-x)}] dx_0 \\ h_e(x, \sigma) &\approx \frac{1}{\sqrt{2}} \left(\int_0^1 e^{-\delta\sigma(1-x_0)} \mathcal{A}_e(T; x_0) dx_0 \right) \\ &\quad \times [e^{\delta\sigma(1-x)} + e^{-3\delta\sigma(1-x)}] - \frac{1}{\sqrt{2}} \int_x^1 \mathcal{A}_e(T; x_0) \\ &\quad \times [e^{\delta\sigma(x_0-x)} + e^{-3\delta\sigma(x_0-x)}] dx_0. \end{aligned} \quad (5.2)$$

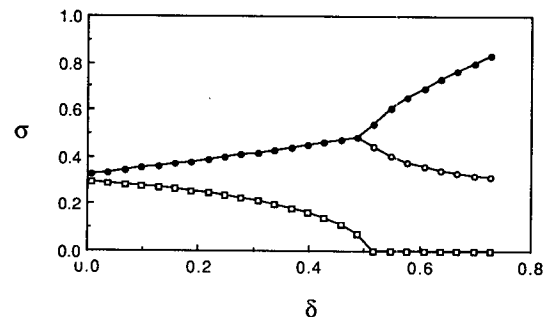


FIG. 7. As in Fig. 6 except for $\epsilon_a = 2.5$ and frequency shown by squares.

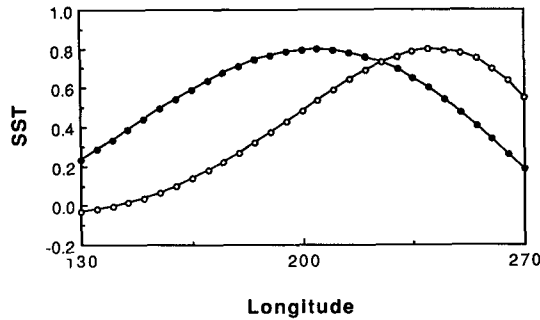


FIG. 8. As in Fig. 5a except with the first-order correction to the fast-wave limit; $\epsilon_a = 1.5$ (solid circles) and $\epsilon_a = 2.5$ (open circles).

The functional approximations for the leading behavior are, of course, not unique. The approximation chosen here satisfies the boundary condition $u_e(1, \sigma) = 0$ and the structure of u_e and h_e clearly indicates that it captures the forced oceanic Kelvin wave and first Rossby wave mode. To make this link, let

$$\begin{aligned} q_e &= h_e + u_e \\ p_e &= h_e - u_e \end{aligned} \quad (5.3)$$

(Gill and Clark 1974) and then invert the integral operator, to obtain

$$\begin{aligned} \delta\sigma q_e + \partial_x q_e &= \sqrt{2} \mathcal{A}_e(T; x) \\ \delta\sigma p_e - \frac{1}{3} \partial_x p_e &= -\frac{\sqrt{2}}{3} \mathcal{A}_e(T; x). \end{aligned} \quad (5.4)$$

It now becomes explicit that the approximation made in (5.2) still retains the information propagation characteristics of the forced Kelvin and first Rossby waves. However, it can be shown that there is about a factor of 1/3 difference in the Rossby wave mode amplitude between the approximation made in (5.2) and what would be obtained by brutal truncation of the wave equation to keep only the Kelvin and first Rossby wave mode. Furthermore, the leading y structure for all terms in (5.2) is $\exp[-y^2/2]$ except in a narrow region of width $O[(\delta\sigma)^{-1}]$ near the eastern boundary. An important feature in the approximation (5.2) is that it also maintains consistency in the boundary conditions. With (5.2), we can easily show that at this level of approximation

$$q_e(0, \sigma) = o(e^{-3\delta\sigma}), \quad (5.5)$$

which indicates that when $\text{Re}(\delta\sigma)$ is large, western boundary reflection is no longer an important process and these waves do not interact to form ocean basin modes. Physically, this is simply because enough growth occurs in the interior solution during the adjustment time that returning wave signals does not affect the leading behavior. In the coupled problem, this implies that the oscillating ocean basin modes will dis-

appear under conditions of strong growth (or weak growth in presence of strong damping).

The eigenvalue problem now consists of the approximate form of the oceanic response, (5.2), together with the SST equation for $\delta_s = 0$, (4.1), and the atmospheric operator, (2.3). The system again forms an integral equation and may be solved by the same method applied in sections 3 and 4. For self-consistent solutions, strongly growing modes must be obtained. By inverting the integral equation, we obtain a dispersion relation:

$$\begin{aligned} (\sigma + \epsilon_w)(k^2 - 2\epsilon_a k - 3\epsilon_a^2)(k + \delta\sigma)(k - 3\delta\sigma) \\ = -2\sqrt{2}\mu\epsilon_a A_0(\gamma(k - \delta\sigma) - 2a\delta\sigma)k, \end{aligned} \quad (5.6)$$

which for each eigenvalue σ gives four roots for k . Thus, the solution can be written as

$$T = \left(\sum_{i=1}^4 T_{k_i} e^{k_i x}\right) e^{\sigma t}. \quad (5.7)$$

Substituting (5.7) back to (4.1) and (5.2), we get the eigenvalue equation:

$$\begin{aligned} \sum_{i=1}^4 T_{k_i} \frac{e^{k_i}}{3\epsilon_a - k_i} &= 0 \\ \sum_{i=1}^4 T_{k_i} \frac{1}{\epsilon_a + k_i} &= 0 \\ \sum_{i=1}^4 T_{k_i} \frac{B(k_i)}{\delta\sigma + k_i} &= 0 \end{aligned}$$

$$\sum_{i=1}^4 T_{k_i} \left(\frac{1}{-3\delta\sigma + k_i} - \frac{1}{\delta\sigma + k_i} \right) B(k_i) e^{k_i} = 0 \quad (5.8)$$

where $B(k_i)$ is defined in (4.7). The first two equations of (5.8) are obtained in the same way as for (3.6). The last two are obtained by demanding that the coefficients of the x -dependent terms $\exp(\delta\sigma x)$ and $\exp(-3\delta\sigma x)$, which come from the oceanic boundary conditions, vanish identically. As always the eigenvalues are given by the condition that the matrix multiplying the eigenvector (T_{k_i}) have zero determinant.

Despite the simplifications, the system (5.6)–(5.8) must still be solved numerically except in certain special cases. The dependence of the gravest strongly growing mode on coupling is shown in Fig. 9 for several values of δ . The curves in Fig. 9 lie within the range of validity of the approximations made in (5.2) when $\delta \text{Re}(\sigma) \gg 1$, which indeed occurs in the region $\mu \gg 1$. The curves continue to behave sensibly even outside the range of validity of the approximation, plotted with crosses for $\delta \text{Re}(\sigma) < 1$ to indicate that they should not be trusted. However, the approximations (7.1) are valid to within 10% (rms error) even for $\delta\sigma = 1$. The mode is purely growing for the range of coupling shown, except for the $\delta = 3$ curve. For this case, a

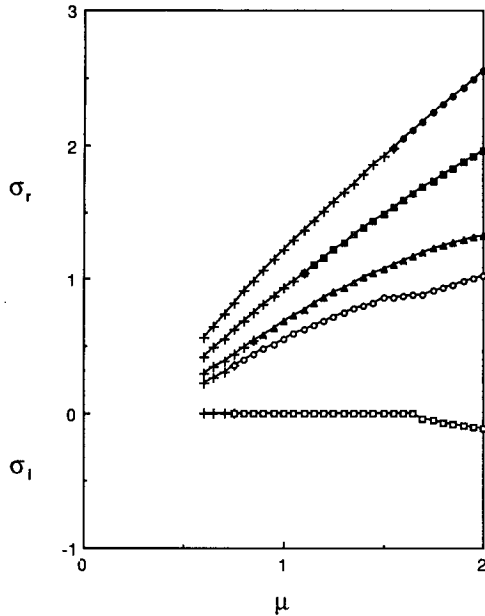


FIG. 9. Growth rate of the gravest stationary growing mode vs coupling, μ , in the strong-coupling limit for $\delta = 0.5$ (solid circles), $\delta = 1.0$ (solid squares), $\delta = 2.0$ (solid triangles), $\delta = 3.0$ (open circles). Open squares for frequency in the case of $\delta = 3.0$. Other parameters: $a = 0.5$, $\gamma = 1.0$, $\epsilon_w = 1.0$, $\epsilon_a = 2.0$. Portions of curves with crosses show μ values for which $\text{Re}(\delta\sigma) \leq 1$, where curves are outside range of validity.

transition to propagation is seen at larger μ , which will be discussed below. In the case nearest the fast-wave limit, $\delta = 0.5$, the growth rate is almost linear in μ for large μ and this property changes only slightly as δ increases, even far from the fast-wave limit. This linearity near the fast-wave limit is just as expected for a mode that matches continuously to the corresponding gravest SST mode at the fast-wave limit.

The SST component of the eigenstructure is shown in Fig. 10. This eigenstructure strongly resembles that of the SST modes near the fast-wave limit when δ is small and changes only slightly as it increases, as may be seen from the $\delta = 1$ case shown. The SST field is trapped in the eastern part of the basin by the same mechanisms discussed in the fast-wave limit. The eigenstructure also changes fairly slowly with coupling, as may be seen from the two μ values shown, and is consistent with the SST structure of the mixed SST/ocean-dynamics modes near the 2-degeneracies found in Part I.

With this further numerical evidence of continuity between the growing modes in the strong-coupling limit and the SST modes in the fast-wave limit, we seek cases of (5.8) in which the analytic solutions can be carried further and that link the solutions to those already obtained in the fast-wave limit. If, in (5.6), we let $\delta \rightarrow 0$, the dispersion relation becomes

$$(\sigma + \epsilon_w)(k^2 - 2\epsilon_a k - 3\epsilon_a^2) = -2\sqrt{2}\mu\epsilon_a A_0. \quad (5.9)$$

The corresponding eigenvalue equation can be written

$$\sum_{i=1}^2 \frac{e^{k_i}}{3\epsilon_a - k_i} T_{k_i} + \frac{1}{3\epsilon_a} T_0 = 0$$

$$\sum_{i=1}^2 \frac{T_{k_i}}{\epsilon_a + k_i} + \frac{T_0}{\epsilon_a} = 0$$

$$\sum_{i=1}^2 \frac{B(k_i)}{k_i} T_{k_i} + \frac{\sigma + \epsilon_w}{\sqrt{2}\gamma\mu\epsilon_a A_0} T_0 = 0. \quad (5.10)$$

Because there are two roots of (5.6)—say, k_3 and k_4 —identically zero, we have dropped T_{k_3} and T_{k_4} from the eigenstructure corresponding to (5.7) and replaced them both with T_0 to denote the constant component. Due to the two zero roots, it is more straightforward to obtain (5.10) by setting $\delta = 0$ in (5.2) than by taking the limit $\delta \rightarrow 0$ in (5.8).

The system (5.9)–(5.10) represents the fast-wave limit of the strong-coupling limit system (5.6)–(5.8), but it should be pointed out that it is not formally an approximation to the original system: (5.6) is derived under the assumption $\text{Re}(\delta\sigma) \gg 1$, which is violated as $\delta \rightarrow 0$. Here we encounter the difficulty that there is formally no region of overlap of the strong coupling and fast-wave limits—they represent almost converse limits in terms of the assumptions regarding $|\delta\sigma|$. However, drawing on the results of section 4, the magnitude of $\delta\sigma$ depends on the product $\delta\mu$ for large coupling, near the fast-wave limit. The regions of validity in parameter space thus approach each other for small δ and large μ as shown in Fig. 1 of Part II. It is thus not surprising that when we push the strong-coupling limit equations beyond their region of validity and into the fast-wave limit, we still get a good qualitative match to the true fast-wave limit equations, (4.8)–(4.9).

The dispersion relation (5.9) is identical in form to that obtained in the fast-wave limit, (4.8). The only difference is a factor of $\sqrt{2}$ multiplying μ . The eigenvalue equations (5.10) differ in the coefficients of the third equation. The similarity of the dispersion relation obtained from these two very different approximations

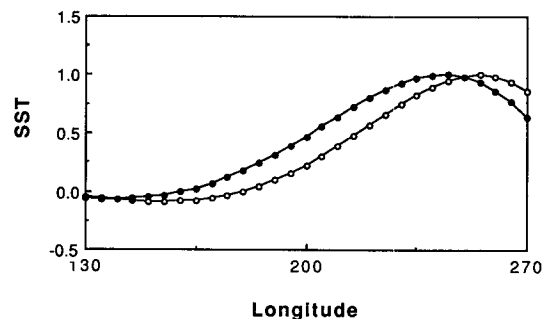


FIG. 10. SST structure of the gravest stationary SST mode in the strong-coupling limit for $\delta = 1.0$, $\mu = 1.0$ (solid circles) and $\mu = 2.0$ (open circles): arbitrary units.

implies the connection of the SST modes in the fast-wave limit and the modes described by the system (4.1) and (5.2). The surviving eigenvalue in (5.9) is that of the SST equation, making it clear that the surface of eigenvalues represented by slices at various values of δ in Fig. 9 indeed approaches an SST mode in the fast-wave limit.

It remains to be verified that the behavior of the modes indeed matches qualitatively that found in the fast-wave limit; the connection implied by the dispersion relation does not alone guarantee this because the boundary conditions arising from the ocean component differ from the true fast-wave limit, as may be seen by comparing the coefficients of the third equation of (5.10) and (4.9). To examine the extent of the differences, we turn first to the case $\delta = 0$ and the approximation of small ϵ_a in the atmospheric structure with $\epsilon_a A_0$ order unity in the magnitude, for which the analytical solution (4.12) was obtained in the fast-wave limit. Applying this case to the strong-coupling limit equations (5.9)–(5.10), we find from the dispersion relation, (5.9),

$$k_1 = -k_2 = i\hat{k},$$

which in (5.10) gives $T_{k_1} = -T_{k_2}$ while $T_0 = O(\epsilon_a)$ is small, and the eigenvalue equation becomes

$$\cos(\hat{k}) = -\frac{1}{3} \tag{5.11}$$

giving

$$\hat{k} = \begin{cases} k_{01} + 2n\pi \\ k_{02} + 2n\pi, \end{cases} \quad n = 0, 1, 2, \dots, \tag{5.12}$$

where $(k_{0i}, i = 1, 2)$ are the first two roots of (5.11). The modes are purely growing, relative to ϵ_w :

$$\sigma = -\epsilon_w + 2\sqrt{2}\mu\hat{k}^{-2}, \tag{5.13}$$

with the gravest mode being the fastest growing. Except for the difference in the value of k_{0i} , the eigenstructures are also very similar to the results in fast-wave limit. Thus, despite the differences in oceanic boundary conditions, and despite the fact that the approximations made in the strong-coupling limit are only valid asymptotically for large $\text{Re}(\delta\sigma)$, the leading behavior obtained from the strong-coupling equations matches smoothly to the fast-wave limit.

We can further check this in the case $\epsilon_a \neq 0$. Similarly as in Fig. 4, Fig. 11 shows the dependence of $\hat{f}(k_1, \epsilon_a)$ and k_1 on ϵ_a , using the same definition of \hat{f} , (4.14). The growth rate of the modes is again linearly proportional to $\hat{f}(k_1, \epsilon_a)$ with a relation almost identical to (4.15):

$$\sigma + \epsilon_w = 2\sqrt{2}\mu\gamma\hat{f}(k_1, \epsilon_a). \tag{5.14}$$

The dependences are very similar before the degeneracy that marks the transition from a stationary to an os-

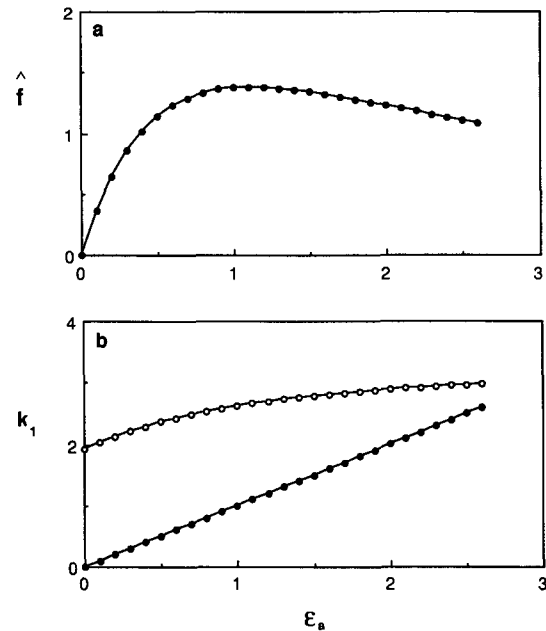


FIG. 11. As in Fig. 4 except in the case of the strong-coupling limit system pushed into the fast-wave limit. Only the gravest mode is shown.

cillatory (eastward propagating) mode in Figs. 4a,b, which is lacking in Fig. 11. The strong-coupling limit version gives only stationary modes at $\delta = 0$. The fact that a strong-coupling limit favors stationary rather than propagating modes when pushed into the fast-wave case may be related to the phenomenon noted in Fig. 7, where ϵ_a was large enough that the gravest mode was propagating in the fast-wave limit but became stationary as δ was increased. At least in the non-propagating range, the similarity of the wavenumbers k_1 (and thus also k_2) for the modes in this fast-wave version of the strong-coupling limit and for those obtained in the true fast-wave limit suggests that the discussion of the east basin trapping effect in the SST eigenstructure given in section 4 should carry over smoothly to the strong-coupling limit.

Having made the case that the strong-coupling limit system gives a suitably behaved SST mode when pushed into the fast-wave limit, we now examine the connection between this and the range in which the strong-coupling approximations are really valid; that is, $\delta > O(\mu^{-1})$. We trace the eigenmodes numerically from $\delta = 0$, starting with values obtained from (5.9)–(5.10), and gradually increasing δ in (5.6)–(5.8). Figure 12 shows for fixed coupling how the eigenvalue changes continuously with δ . Although the region with small δ is well outside the range of validity of this approximation, it remains well behaved. Comparing with Fig. 6, which is valid for small δ , it may be seen that the strong-coupling limit solution of Fig. 12 does incur an error in this region but that the results of the two

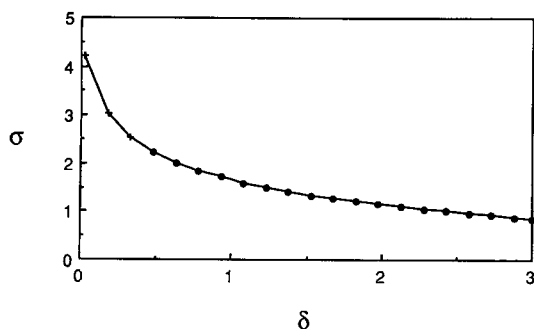


FIG. 12. Growth rate of the gravest stationary SST mode vs δ in the strong coupling limit with $a = 0.5$, $\gamma = 1.0$, $\epsilon_w = 1.0$, $\epsilon_a = 1.5$, $\mu = 1.5$. Portion of curve with $\text{Re}(\delta\sigma) \leq 1$ is shown by crosses.

approximations approach each other for moderate δ . Unfortunately, there is no asymptotic matching region, so the approximations from the two ends do not overlap smoothly. The closeness of the two curves in the middle provides an indication of where the curve in Fig. 12 becomes a qualitative rather than quantitative representation of the eigensurface of the full system. Our argument in this case thus must depend primarily on the *form* of the eigenvalue equations in (5.9)–(5.10) and the physical interpretation of the eigenvalue.

This connection between the SST modes in the fast-wave limit and the stationary growing modes at finite δ can be continued all the way to the fast-SST limit. To do so, we rescale time by a combined SST plus dynamical time scale, so the eigenvalue is rescaled by $(1 + \delta)$, and introduce the modified relative time scale parameter, $\delta^* \equiv \delta/(1 + \delta)$, as outlined in section 3 of Part II. The fast-wave limit still occurs at $\delta^* = 0$ but the fast-SST limit is now at $\delta^* = 1$ in the transformed parameter plane. Figure 13 shows the eigenvalues of the two gravest modes traced from the fast-wave limit to the fast-SST limit in these coordinates, under the strong-coupling approximation. Both modes remain purely growing and show little qualitative change over the whole domain. This connection is remarkable considering that only the SST-equation time derivative is important to the mode at one end and only an ocean-related time derivative is important at the other end.

We also observe dependency on the atmospheric damping length in the fast-SST limit similar to that found in the fast-wave limit. Figure 14 shows the two gravest modes as a function of ϵ_a in this case, exhibiting the merger of the two stationary modes into a propagating pair, in a manner similar to Fig. 4. The value of ϵ_a for which this transition to propagation occurs depends on the values of μ and δ . The same surface of 2-degeneracies was seen in Fig. 9 for the $\delta = 3$ curve for a slice in the μ direction. We suspect that this behavior also carries over from the fast-SST limit to the fast-wave limit in a relatively straightforward manner, but we have not pursued it since it does not seem to be a crucial aspect of the problem.

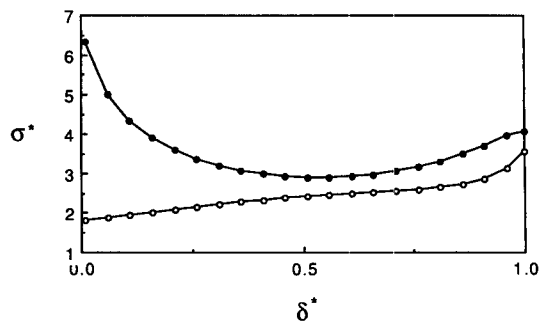


FIG. 13. Rescaled growth rate of the two gravest stationary SST modes vs δ^* in the strong-coupling limit with $a = 0.5$, $\gamma = 1.0$, $\epsilon_w = 1.0$, $\epsilon_a = 1.0$, $\mu = 2.0$. Solid circles for the first mode, open circles for the second.

The models of Cane et al. (1990, hereafter CMZ) and Schopf and Suarez (1990, hereafter SS90) are formulated in the fast-SST limit in a manner very similar to a special case of the present model: that in which the coefficients γ and ϵ_w are assumed large and to have a delta-function spatial structure in x . Thus, they exclude the possibility of a sequence of modes associated with a set of spatial structures of SST, the possibility of propagating modes and the possibility of destabilizing mechanisms other than the thermocline feedback. The lowest-frequency mode does offer a qualitative approximation to the gravest mode discussed above, in the regime in which it exhibits stationary growth in the strong-coupling limit and connects to an ocean basin mode in the weak-coupling limit. In CMZ (their Figs. 1–5), the 2-degeneracy associated with the connection of the stationary growing mode at strong coupling and the mixed mode with subsurface memory is clearly seen, consistent with the 2-degeneracy extending from the 3-degeneracy at order unity values of δ all the way to the fast-SST limit. From the results above, it is clear that this transition from oscillatory behavior related to wave time scales to pure growth is associated with the onset of the strong-coupling limit and that this tran-

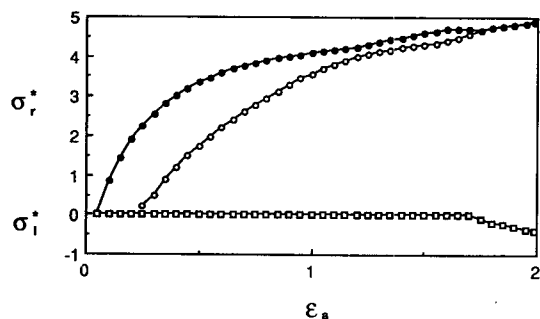


FIG. 14. Rescaled growth rate (solid circles for the first mode, open circles for the second) and frequency (squares) of the two gravest modes vs ϵ_a in the strong-coupling and fast-SST limit with $a = 0$, $\gamma = 1.0$, $\epsilon_w = 1.0$, $\delta^* = 1.0$, $\mu = 2.0$.

sition occurs under quite general conditions. Knowing that the pure-growth branch connects directly to an SST mode in the fast-wave limit removes the mystery of how these models relate, for instance, to that of Battisti and Hirst (1989), in which estimates were based on the SST equation: the CMZ and SS90 models simply approximate from the fast-SST limit one branch of the set of connected eigensurfaces for the gravest mixed SST/ocean-dynamics modes discussed in Part I. The growth and spatial characteristics of this eigensurface are strongly related to those of the gravest stationary SST mode, for sufficiently strong coupling.

6. Summary and discussion

Much of the dynamics of the coupled tropical ocean-atmosphere system including the primary bifurcation, which tends to determine the character of interannual variability (e.g., Neelin 1990; Münnich et al. 1991), may be understood via the eigenmodes of the system linearized about a climatological basic state. The parameter dependence of these modes is of interest both as a means of understanding how the coupled modes are constructed and because it can explain the sensitivity exhibited by simple and intermediate coupled models (e.g., Philander et al. 1984; Cane and Zebiak 1985; Hirst 1988; Schopf and Suarez 1988, 1990; Battisti and Hirst 1989; Graham and White 1990; Wakata and Sarachik 1991; Cane et al. 1990; Neelin 1991) and by coupled GCMs (e.g., Neelin et al. 1992). In Part I of this series, we showed numerically how the two ingredients that are familiar from the uncoupled problem—SST modes and ocean dynamics modes—merge in the coupled parameter space. The analytical or near-analytical results of Parts II and III, which provide physical insight into the coupled modes and an indication of the robustness of the numerical results, are summarized here.

A formulation of the coupled eigenvalue problem in a finite basin was outlined in Part II which is particularly useful as a basis for making approximations. From this, we obtain results in several limits that almost completely surround the order-unity region of parameter space, which both exhibits complex behavior and best applies to the real coupled system. Our strategy is to attempt to delineate a global picture of the behavior by piecing these results together. The following limits and cases were considered.

1) *The weak-coupling limit.* In Part II, we examined series solutions in μ , beginning with the uncoupled modes at zeroth order, whose radius of convergence encompasses a significant range of coupling values. In the case of the SST modes, the effects of coupling dominate the structure of the mode even at very weak coupling, when the eigenvalue correction is still small. The uncoupled modes for the ocean dynamics are the ocean basin modes of Cane and Moore (1981), plus a scattering spectrum. Examining the coupled mode corre-

sponding to the gravest ocean basin mode, we find that it retains its resemblance to the uncoupled version through a modest range of coupling but rapidly takes on a mixed character as coupling is increased, producing lower frequency and positive growth rates. The value of coupling at which the modification of the structure begins to have strong effects on the eigenvalue provides a measure of where the mode can no longer be thought of as a weakly coupled ocean basin mode and must be considered a mixed SST/ocean-dynamics mode.

2) *Case of surface-layer processes only.* The interaction of SST and perturbation currents due to Ekman drift processes in the active surface layer tends to give westward-propagating SST modes. The case with only these processes is simple in that it involves only atmospheric boundary conditions in the finite basin and so provides a transparent example of the solution method. For the case where the atmospheric damping length scale is large (small ϵ_a), and coefficients are zonally constant within the basin, fully analytic solutions show that there is a countably infinite set of nonorthogonal, westward-propagating modes of which the gravest is the lowest-frequency and most unstable mode. When ϵ_a is of realistic magnitude, the mode does not change qualitatively. Without zonal variations in the basic state, these modes tend to have significant amplitude through most of the basin.

3) *Fast-wave limit.* The finite basin version of the fast-wave limit can yield growing, stationary SST modes over a significant range of parameters. We focus on these since in the parameter range where propagation occurs, the mechanisms can be qualitatively understood from the periodic basin case of N91. In the small- ϵ_a , constant coefficient case, analytic solutions yield a quantized series of purely growing modes. The gravest spatial mode is the most unstable, and the important characteristic of larger amplitude in the eastern part of the basin is found even in this simple case. For finite ϵ_a , additional eastward trapping occurs at the atmospheric length scale. The east-west asymmetry due to β produces this, with both the atmospheric and oceanic dynamics contributing, although the atmosphere is the more important for realistic parameters. The spatial characteristics of the SST mode in the fast-wave limit carry over into cases where wave time scales can be important, so qualitatively the same mechanism applies to those cases. Because the eastward trapping is a dynamical effect, and does not essentially depend on the zonal variations of the basic state, it is tempting to speculate that a related mechanism may provide the fundamental reason for why the cold tongue occurs in the central and eastern Pacific in the observed climatology. The robustness of the eastward trapping within this parameter range provides support for models such as Cane et al. (1990) that assume it. We also derive a next-order extension to the fast-wave limit to provide a connection to the parameter range where the oceanic

adjustment time can be important. The fast-wave limit is a good approximation even to order-unity relative adjustment times at low coupling, but has a smaller range of validity at high coupling.

4) *Strong-coupling limit.* When coupling is strong enough, it tends to dominate over wave propagation effects in ocean balances. A very interesting approximation is obtained that retains the leading “wave-related” terms. Strongly growing, stationary eigenmodes are found for reasonable values of the relative adjustment time coefficient. These modes depend both on the time derivatives from the SST equation and those from the shallow-water ocean equations but are dominated by coupling, rather than by wave effects. At the fast-wave limit, these solution branches join smoothly onto the SST modes. Considered from a geometric point of view, with eigenvalues forming continuous sheets in parameter space, this joining appears inevitable, at least for the gravest mode, given the behavior in the respective limits.

Once the connection of SST modes and modes with dependence on oceanic time derivatives is made at strong coupling, the question is how the merger arises between these and the oscillatory mixed mode examined in the weak-coupling limit, thus connecting the ocean basin mode eigensurface with the SST mode eigensurface. This involves the degeneracies of multiplicity two and three discussed in Part I; these occur in the region of parameter space in between the regions of validity of the limits discussed above, making an analytical solution difficult. However, the connection of the oscillatory mixed mode to the stationary growing modes is strongly implied by the nature of the strong-coupling limit. The growth rate of any mode whose period depends on wave reflection cannot be too large. If so, the balances appropriate to the strong-coupling limit come to dominate over wave processes, and it will tend to become stationary. This suggests that the 2-degeneracy marking the transition between the low-coupling region where wave time scales can produce oscillation and the strong-coupling region will be a very robust feature of the coupled system. We note that this also implies that a model with overly large oceanic damping cannot have oscillations associated with wave delay; as oceanic damping is increased, coupling can be increased to keep the system above or near its primary bifurcation, but beyond the codimension two bifurcation corresponding to the 2-degeneracy, the bifurcation will be stationary rather than oscillatory.

Extrapolating the results from the various limits toward the central region of parameter space thus gives a consistent global picture of the coupled modes in the μ - δ parameter plane. To complete the understanding of the coupled system, at least a third dimension to the parameter space is needed, governing the transition between stationary and propagating SST modes. We have provided an indication of this using the relative

surface-layer coefficient, δ_s , and the atmospheric damping length parameter, ϵ_a , in subsections of parameter space, although the full volume of the three-dimensional parameter space has not yet been fully mapped out. Analytically, we cannot say much about the $\delta_s = O(1)$ case away from the fast-wave limit. However, it is inevitable that there will be a region in which both wave time scales and processes tending to produce propagation of SST will play a role such as was found in Part I. We hypothesize that this is the region that best corresponds to the observed system.

We argue that the several theoretical conceptions of coupled interannual oscillations (as well as the various regimes of behavior found in numerical coupled models) may all be viewed in a unified manner by thinking of the modes in question as closely related mixed SST/ocean-dynamics modes with a parameter space dependence similar to that presented here. Since the most unstable mode is usually one of the branches of the set of interconnected, spatially gravest mixed modes, it is likely that most of the models in which a single mode of interannual variability is found simply exhibit versions of this in various regimes of behavior. The stationary SST modes near the fast-wave limit provide a good point of departure for conceptual understanding of these neighboring regimes. They provide analytically tractable prototypes for fully coupled modes, in which the multiple coupled feedback mechanisms may be examined. The most important regimes of behavior occur nearby, in the sense that a finite but small change of parameters leads from the purely growing SST modes to oscillation through different mechanisms, while leaving the growth rate and spatial structure characteristics of the modes fundamentally unchanged. Regimes with large eastward-trapped stationary SST components with oscillation time scales set by smaller westward- or eastward-propagating components are reached by small changes, for instance, in δ_s and ϵ_a . The important “standing oscillation regime” is characterized by a standing oscillation in the SST component that has spatial structure nearly identical to that of the stationary SST mode, while ocean dynamical time scales are responsible for the oscillation. It may be reached from the stationary SST mode regime by small changes along appropriate paths in the (δ, μ) plane. We suggest that it is productive to view this standing oscillation mode as a stationary SST mode perturbed by wave time scale effects. As discussed in Part I, this is qualitatively consistent with the view that inspired the heuristic differential delay SST equation, or “delayed oscillator” model, used by Schopf and Suarez (1988) and Battisti and Hirst (1989) to describe coupled behavior in this regime (although there are severe limits on how far the analogy between the toy model and the full eigenvalue problem can be stretched). In the real coupled system, secular or stochastic changes of the parameters by external processes will cause the system to wander between this regime

and neighboring ones, in particular those that include propagation effects. There are a number of GCM results (Latif and Flügel 1991; Philander et al. 1992; Nagai et al. 1992; Latif et al. 1993a,b) and indications from observations (Latif et al. 1993b) that important effects from time scales of subsurface dynamics can indeed occur in combination with propagating features that modify an almost-standing oscillation pattern in SST.

We now offer a few speculations on areas we have touched on but not fully explored. Although we have focused on the spatially gravest modes, there are also possible roles for higher zonal modes, of which we have provided some examples in the simplest cases. When more than one type of variability is observed in a model, it may be due either to the second branch of the set of gravest mixed modes or to higher zonal modes being excited by stochastic forcing or participating in a secondary bifurcation (assuming the first bifurcation does not qualitatively change the assumptions used in this analysis). Higher zonal SST modes may also be involved in coupled aspects of the seasonal cycle through forcing or frequency locking. This might explain the westward propagation of SST and zonal wind in the seasonal cycle in the eastern Pacific (Philander 1991, personal communication). The presence of multiple modes of similar growth rate and of corresponding codimension two bifurcations in sections of parameter space also raises the obvious question of modal interactions in the nonlinear case, some examples of which are found in Hao et al. (1993). The higher zonal modes also have potential impact on the initial growth of disturbances due to the fact that the modes are not orthogonal in this non-self-adjoint system (Blumenthal 1991; Farrel 1989; Zhang 1988). The degeneracies of multiplicity two and three encountered in the system are obvious, extreme examples of this nonorthogonality.

We conclude by suggesting that we now have a fairly complete framework for understanding the linear and weakly nonlinear coupled modes of most current tropical ocean-atmosphere models, especially those related to the Cane and Zebiak model. This provides physical insight into the balances between the multiple mechanisms that can affect the primary bifurcation giving rise to interannual variability. It also lays the groundwork for understanding the cases of linear stochastically forced response and the initial value problem, which should yield insight into the predictability of the system and sources of error growth (Cane et al. 1986; Barnett et al. 1988; Goswami and Shukla 1991). The prototypes of coupled modes in simplifying limits further offer an alternative to intuition based on the largely irrelevant modes of the uncoupled problem in interpreting coupled model results. However, the potentially important effects of the seasonal cycle on these modes have yet to be examined, and open questions remain on the nature and effects of higher bifurcations (e.g., Ghil et al. 1991) and on the role of coupled interactions

in establishing the climatological state and seasonal cycle. We remain aware that the observed system has many features (e.g., Barnett 1983; Wright et al. 1988; Rasmusson et al. 1990; Barnett 1991; Trenberth 1991; Webster and Yang 1992) even more complex than the already dazzling array of mechanisms exhibited by the models.

Acknowledgments. This work was supported in part by NSF Grants ATM-8905164 (JDN), ATM-9013217 (FFJ), and ATM-9215090 (FFJ and JDN), and by NOAA Grant NA16RC0178-01 (FFJ and JDN). The views expressed herein are those of the authors and do not necessarily reflect those of NOAA or its subagencies. C. Wong provided much help in typesetting successive versions of the manuscript. It is a pleasure to acknowledge discussions with D. Battisti, T. Barnett, M. Cane, P. Gent, H. Dijkstra, Z. Hao, I. Held, M. Latif, J. McWilliams, R. Miller, G. Philander, E. Sarachik, P. Schopf, and J. Tribbia, and with J. Pedlosky, whose questions prompted the section on the source of east basin trapping. We particularly thank M. Ghil for much encouragement and support. An earlier version of part of this work appeared in the *Proceedings of the Eighth Conference on Atmospheric Waves and Stability*, American Meteorological Society, 1991.

REFERENCES

- Barnett, T. P., 1983: Interaction of the monsoon and Pacific Trade Wind system at interannual time scales. Part I: The equatorial zone. *Mon. Wea. Rev.*, **111**, 756-773.
- , 1991: The interaction of multiple time scales in the tropical climate system. *J. Climate*, **4**, 269-285.
- , N. Graham, M. Cane, S. Zebiak, S. Dolan, J. O'Brien, and D. Legler, 1988: On the prediction of El Niño of 1986-1987. *Science*, **241**, 192-196.
- , M. Latif, E. Kirk, and E. Roeckner, 1991: On ENSO physics. *J. Climate*, **4**, 487-515.
- Battisti, D. S., 1988: The dynamics and thermodynamics of a warming event in a coupled tropical atmosphere/ocean model. *J. Atmos. Sci.*, **45**, 2889-2919.
- , and A. C. Hirst, 1988: Interannual variability in the tropical atmosphere/ocean system: influence of the basic state and ocean geometry. *J. Atmos. Sci.*, **45**, 1687-1712.
- Blumenthal, M. B., 1991: Predictability of a coupled ocean-atmosphere model. *J. Climate*, **4**, 766-784.
- Cane, M. A., and D. W. Moore, 1981: A note on low-frequency equatorial basin modes. *J. Phys. Oceanogr.*, **11**, 1578-1584.
- , and E. S. Sarachik, 1981: The response of a linear baroclinic equatorial ocean to periodic forcing. *J. Mar. Res.*, **39**, 651-693.
- , and S. E. Zebiak, 1985: A theory for El Niño and the Southern Oscillation. *Science*, **228**, 1084-1087.
- , —, and S. C. Dolan, 1986: Experimental forecasts of El Niño. *Nature*, **321**, 827-832.
- , M. Münnich, and S. E. Zebiak, 1990: A study of self-excited oscillations of the tropical ocean-atmosphere system. Part I: Linear analysis. *J. Atmos. Sci.*, **47**, 1562-1577.
- Farrel, B. F., 1990: Small error dynamics and the predictability of atmospheric flows. *J. Atmos. Sci.*, **47**, 2409-2416.
- Ghil, M., M. Kimoto, and J. D. Neelin, 1991: Nonlinear dynamics and predictability in the atmospheric sciences. *Rev. Geophys. (Suppl)*, 46-55. [U.S. National Report to the International Union of Geodesy and Geophys, 1987-1990.]
- Gill, A. E., 1980: Some simple solutions for heat induced tropical circulation. *Quart. J. Roy. Meteor. Soc.*, **106**, 447-462.

- , and A. J. Clarke, 1974: Wind-induced upwelling, coastal current, and sea-level changes. *Deep-Sea Res.*, **21**, 325–345.
- Goswami, B. N., and J. Shukla, 1991: Predictability of a coupled ocean–atmosphere model. *J. Climate*, **4**, 3–22.
- Graham, N. E., and W. B. White, 1990: The role of the western boundary in the ENSO cycle: Experiments with coupled models. *J. Phys. Oceanogr.*, **20**, 1935–1948.
- Hao, B., J. D. Neelin, and F.-F. Jin, 1993: Nonlinear tropical air–sea interaction in the fast-wave limit. *J. Climate*, **6**, 1523–1544.
- Hirst, A. C., 1988: Slow instabilities in tropical ocean basin–global atmosphere models. *J. Atmos. Sci.*, **45**, 830–852.
- Jin, F.-F., and J. D. Neelin, 1993: Modes of interannual tropical ocean–atmosphere interaction—a unified view. Part I: Numerical results. *J. Atmos. Sci.*, **50**, 3477–3503.
- Latif, M., and M. Flügel, 1991: An investigation of short-range climate predictability in the tropical Pacific. *J. Geophys. Res.*, **96**, 2661–2673.
- , A. Sterl, E. Maier-Reimer, and M. M. Junge, 1992a: Climate variability in a coupled GCM. Part I: the tropical Pacific. *J. Climate*, **6**, 5–21.
- , —, —, and —, 1993b: Structure and predictability of the El Niño/Southern Oscillation phenomenon in a coupled ocean–atmosphere general circulation model. *J. Climate*, **6**, 700–708.
- Lau, N. C., S. G. H. Philander, and M. J. Nath, 1992: Simulation of El Niño/Southern Oscillation phenomena with a low-resolution coupled general circulation model of the global ocean and atmosphere. *J. Climate*, **5**, 284–307.
- Meehl, G. A., 1990: Seasonal cycle forcing of El Niño–Southern Oscillation in a global coupled ocean–atmosphere GCM. *J. Climate*, **3**, 72–98.
- Münnich, M., M. A. Cane, and S. E. Zebiak, 1991: A study of self-excited oscillations in a tropical ocean–atmosphere system. Part II: Nonlinear cases. *J. Atmos. Sci.*, **48**, 1238–1248.
- Nagai, T., T. Tokioka, M. Endoh, and Y. Kitamura, 1992: El Niño/Southern oscillation simulated in an MRI atmosphere–ocean coupled general circulation model. *J. Climate*, **1202**–1233.
- Neelin, J. D., 1990: A hybrid coupled general circulation model for El Niño studies. *J. Atmos. Sci.*, **47**, 674–693.
- , 1991: The slow sea surface temperature mode and the fast-wave limit: Analytic theory for tropical interannual oscillations and experiments in a hybrid coupled model. *J. Atmos. Sci.*, **48**, 584–606.
- , and F.-F. Jin, 1993: Modes of interannual tropical ocean–atmosphere interaction—a unified view. Part II: Analytical results in the weak-coupling limit. *J. Atmos. Sci.*, **50**, 3504–3522.
- , M. Latif, M. A. F. Allaart, M. A. Cane, U. Cubasch, W. L. Gates, P. R. Gent, M. Ghil, C. Gordon, N. C. Lau, C. R. Mechoso, G. A. Meehl, J. M. Oberhuber, S. G. H. Philander, P. S. Schopf, K. R. Sperber, T. Tokioka, J. Tribbia, and S. E. Zebiak, 1992: Tropical air–sea interaction in general circulation models. *Climate Dyn.*, **7**, 73–104.
- Philander, S. G. H., T. Yamagata, and R. C. Pacanowski, 1984: Unstable air–sea interactions in the tropics. *J. Atmos. Sci.*, **41**, 604–613.
- , R. C. Pacanowski, N. C. Lau, and M. J. Nath, 1992: A simulation of the Southern Oscillation with a global atmospheric GCM coupled to a high-resolution, tropical Pacific ocean GCM. *J. Climate*, **5**, 308–329.
- Rasmusson, E. M., X. Wang, and C. F. Ropelewski, 1990: The biennial component of ENSO variability. *J. Mar. Syst.*, **1**, 71–96.
- Schopf, P. S., and M. J. Suarez, 1988: Vacillations in a coupled ocean–atmosphere model. *J. Atmos. Sci.*, **45**, 549–566.
- , and —, 1990: Ocean wave dynamics and the time scale of ENSO. *J. Phys. Oceanogr.*, **20**, 629–645.
- Trenberth, K. E., 1991: General characteristics of El Niño–Southern Oscillation. *Teleconnections Linking Worldwide Climate Anomalies*. M. Glantz, R. W. Katz and N. Nicholls, Eds., Cambridge University Press, 13–42.
- Wakata, Y., and E. S. Sarachik, 1991: Unstable coupled atmosphere–ocean basin modes in the presence of a spatially varying basic state. *J. Atmos. Sci.*, **48**, 2060–2077.
- Webster, P. J., and S. Yang, 1992: Monsoon and ENSO: Selectively interactive systems. *Quart. J. Roy. Meteor. Soc.*, **118**, 877–926.
- Wright, P. B., J. M. Wallace, T. P. Mitchell, and C. Deser, 1988: Correlation structure of the El Niño/Southern Oscillation phenomenon. *J. Climate*, **1**, 609–625.
- Zebiak, S. E., and M. A. Cane, 1987: A model El Niño Southern Oscillation. *Mon. Wea. Rev.*, **115**, 2262–2278.
- Zhang, Z., 1988: The linear study of zonally asymmetric barotropic flows. Ph.D. thesis. Reading University, 178 pp. [Available from The British Library, Boston Spa, United Kingdom LS23 7BQ.]